Loss Development Analysis of a Micro-Scale Centrifugal Compressor

Jonna Tiainen[a,*], Ahti Jaatinen-Värri[a], Aki Grönman[a], Tore Fischer[b], Jari Backman[a]

[a] *Laboratory of Fluid Dynamics, School of Energy Systems, Lappeenranta University of Technology, P.O. Box 20, FI-53851 Lappeenranta, Finland*
[b] *Institute of Turbomachinery and Fluid Dynamics, Leibniz Universität Hannover, Appelstraße 9, D-30167 Hannover, Germany*

Abstract

The ever-increasing demand for more efficient energy conversion has placed designers under increasing pressure to develop processing equipment that can meet contemporary needs. It has long been known that a decreasing Reynolds number has a negative effect on centrifugal compressor efficiency. The drop in efficiency can be accounted for relatively easily in the design process using various empirical correlations. However, the correlations only account for a reduction in performance; they do not offer any consideration of the extent to how the drop in efficiency can be countered in the design process. To identify potential methods by which it is possible to improve the performance of centrifugal compressors operating at low Reynolds numbers, the loss development in centrifugal compressors with a reducing Reynolds number must be studied. Recent works on loss development, in general, have focused on the overall performance deterioration, and the differentia-

*Corresponding author
Email address: `jonna.tiainen@lut.fi` (Jonna Tiainen)

tion of the losses originating from different causes with the reducing Reynolds number has been studied only in an axial compressor. The present paper examines loss development in a centrifugal compressor with a vaneless diffuser with respect to the Reynolds number and differentiates between the losses that originate from different causes. A new hybrid method is used to calculate the boundary layer thickness inside a complex flow field. The results show that the diffuser plays a significant role in the performance deterioration of centrifugal compressors with a low Reynolds number and should be included in the loss development analysis. A study of the boundary layers, flow fields and loss development indicates that growth in the impeller hub and diffuser boundary layers should be reduced to improve the performance of the compressor.

Keywords: boundary layer thickness, CFD, correction equation, low Reynolds number, tip clearance, transition

---

Nomenclature

Latin alphabet

A	area	[m^2]
a	fraction of Reynolds-number-independent losses in Eqn. (2)	[-]
a	speed of sound	[m/s]
b	blade height	[m]
b	fraction of Reynolds-number-dependent losses in Eqn. (4)	[-]
B_{ref}	coefficient in Eqns. (5) and (6)	[-]
c	absolute velocity	[m/s]
c	chord length	[m]

c	coefficient in Eqn. (3)	[-]
c_f	friction coefficient	[-]
C_pr	pressure recovery coefficient	[-]
c_p	specific heat capacity at constant pressure	[J/kgK]
D	diameter	[m]
f	friction factor	[-]
h	specific enthalpy	[J/kg]
K_p	total pressure loss coefficient	[-]
Ma_U	tip speed Mach number	[-]
n	Reynolds-number-ratio exponent in Eqns. (2) and (4)	[-]
n	rotational speed	[rpm]
N_s	specific speed	[-]
p	pressure	[Pa]
q_m	mass flow rate	[kg/s]
q_v	volume flow rate	[m^3/s]
R	specific gas constant	[J/kgK]
r	radius	[m]
Re_c	chord Reynolds number	[-]
T	temperature	[K]
t	tip clearance	[m]
U	tip speed	[m/s]
U_δ	velocity at the boundary layer edge	[m/s]
U_∞	free-stream velocity	[m/s]
w	relative velocity	[m/s]

Greek alphabet

α	flow angle	[°]
δ	boundary layer thickness	[m]
η	efficiency	[-]
μ_0	work input coefficient	[-]
ν	kinematic viscosity	[m^2/s]
ω	angular velocity	[rad/s]
ϕ	flow coefficient	[-]
π	pressure ratio	[-]
ψ	pressure coefficient	[-]
ρ	density	[kg/m^3]

Abbreviations

DES	design point
FB	full blade
LE	leading edge
NC	near choke
NS	near stall
PE	peak efficiency point
PS	pressure side
SB	splitter blade
SF	scaling factor
SS	suction side
TE	trailing edge

Subscripts

1	impeller inlet
2	impeller outlet

3	diffuser outlet
ave	average
crit	critical
r	radial
ref	baseline case
s	isentropic, static
t	total

1. Introduction

The sustainable development goals of the United Nations aims at reducing greenhouse gas emissions, improving energy efficiency and increasing the share of renewable energy sources [1]. Additionally, the European Union has similar goals [2]. Finland has committed to the EU targets and aims at increasing self-sufficiency in energy [3]. The industrial sector accounts for, on average, 50% of the overall electricity consumption [4]. A cost-effective way to achieve the international and national targets involves improving energy efficiency [5]. The improvement of compressor performance, in particular, plays an important role in improving energy efficiency and reducing the end-use electricity demand, as compressors alone account for 15% of the overall electricity consumption within industry [4].

Micro-scale centrifugal compressors (impeller outlet diameter less than 30 mm [6]) have great potential for efficiency improvement due to their clearly low performance. The performance of micro-scale centrifugal compressors is worse than that of the larger compressors due to the losses caused by low Reynolds numbers, the larger relative blade thickness, surface roughness and tip clearance [7]. The effect of Reynolds number on the compressor performance was discovered e.g. by Yang et al. [8].

The improvement in the efficiency of the micro-scale centrifugal compressors could result in e.g. the increased technological feasibility of micro-scale gas turbines [9]. Micro-scale gas turbines (less than 100-1,000 kW [10]) could represent a potential solution for combined heat and power applications to cut greenhouse gas emissions [11]. These machines are both flexible and scalable [12]. Therefore, they could also increase the share of renewable energy sources and self-sufficiency in energy [9]. In addition to distributed energy generation, micro-scale gas turbines also hold potential in applications that require a compact, portable power source due to high power density; e.g., unmanned aerial vehicles [13]. A micro-scale centrifugal compressor could also replace a displacement compressor in small refrigeration systems to achieve lower power consumption and weight [14].

The effect of the Reynolds number on the compressor efficiency can be accounted for relatively easily in the design process with empirical correction equations; however, these equations do not consider whether the efficiency drop can be countered somehow. Thus, in order to find potential ways to improve the performance of low-Reynolds-number compressors, loss development in centrifugal compressors with reducing Reynolds number is studied in this paper.

Recent works on loss development in low-Reynolds-number compressors have, in general, focused on the overall performance deterioration in the compressor stage. In a centrifugal compressor, the results of Schleer and Abhari [15] showed a 0.5% decrease in the total-to-static pressure ratio. In addition, the results of Zheng et al. [16] showed a 6.9% decrease in the total-to-total isentropic efficiency of a centrifugal compressor. In an axial compressor, the study of Choi et al. [17] indicated approximately a 69% increase in the total pressure loss coefficient. In addition to the total pressure loss, Choi et al. [17] investigated the differentiation of losses originating from different causes with the reducing Reynolds number in the axial compressor. To the author's best knowledge, the differentiation of losses with the reducing Reynolds number has not previously been investigated in centrifugal compressors apart from the previous work by the authors, where the loss development was studied in the downscaled centrifugal compressors [18]. And later in the centrifugal compressors with varying inlet conditions [19].

The above-mentioned recent works on the differentiation of losses in low-Reynolds-number centrifugal compressors have focused on the impeller, while considerably less attention has been placed on the diffuser. This is because, according to Dietmann and Casey [20], more losses occur in the impeller than in the diffuser due to higher velocities. The hypothesis of this work is that the diffuser plays a marked role in the performance deterioration of the compressor. Thus, the first novel aspect of this study is that the role of a vaneless diffuser in the loss development is analysed. The second novel aspect of the study is that it demonstrates how the hybrid method [21] for calculating the boundary layer thickness inside the complex flow field of a centrifugal compressor enables a more sophisticated analysis of the losses associated with the blade and endwall boundary layers from the impeller inlet to the diffuser outlet than in previous works by the authors. Additionally, the question of whether the transition model should be used when modelling

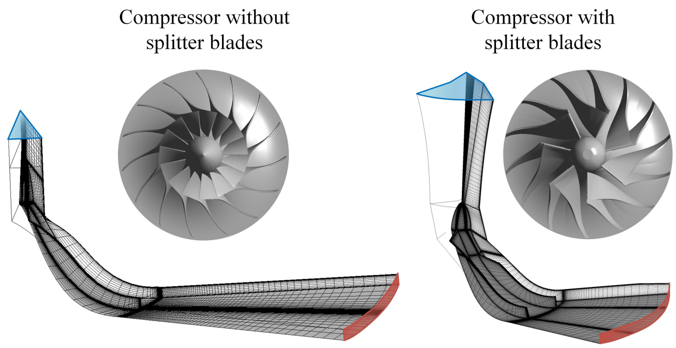

Figure 1: Compressor geometries and computational domains

the low-Reynolds-number centrifugal compressors is addressed in this paper.

2. Methods

The effect of the Reynolds number on centrifugal compressor performance and losses were assessed in two centrifugal compressors: one with splitter blades and the other without. The compressor geometries and computational domains are shown in Fig. 1. Both compressors included a vaneless diffuser. The compressor with splitter blades was studied experimentally and numerically at Lappeenranta University of Technology, Finland [22]. The compressor without splitter blades is the test case Radiver, for which the measurements were carried out at the Institute of Jet Propulsion and Turbomachinery at RWTH Aachen, Germany. Part of the research was funded by the Deutsche Forschungsgemeinschaft (DFG) [23]. The compressor with splitter blades was studied at the design point and the compressor without splitter blades at the peak efficiency point at a reduced speed, $n/n_{\mathrm{DES}} = 0.8$. Details of the compressor geometries and the significant dimensionless per-

Table 1: Technical data of the compressors

	With splitter blades	Without splitter blades
Number of blades	7 + 7	15
Relative blade height (b_2/D_2)	0.058	0.041
Relative tip clearance (t/b_2)	0.052	0.045
Chord Reynolds number ($Re_\mathrm{c} = \frac{w_1 c}{\nu_1}$)	$17 \cdot 10^5$	$16 \cdot 10^5$
Flow coefficient ($\phi = \frac{q_\mathrm{v}}{U_2 D_2^2}$)	0.065	0.051
Pressure coefficient ($\psi = \frac{\Delta h_\mathrm{s}}{U_2^2}$)	0.520	0.450
Specific speed ($N_\mathrm{s} = \frac{\omega\sqrt{q_\mathrm{v}}}{\Delta h_\mathrm{s}^{0.75}}$)	0.830	0.830
Tip speed Mach number ($Ma_\mathrm{U} = \frac{U_2}{a_1}$)	0.920	1.170

formance parameters at the design/peak efficiency point are shown in Table 1.

Both compressors were modelled at three different operating points: the one with splitter blades at the design operating point ($q_\mathrm{m}/q_\mathrm{m,DES} = 1.0$, $n/n_\mathrm{DES} = 1.0$), near choke ($q_\mathrm{m}/q_\mathrm{m,DES} = 1.3$, $n/n_\mathrm{DES} = 1.0$) and near stall ($q_\mathrm{m}/q_\mathrm{m,DES} = 0.6$, $n/n_\mathrm{DES} = 1.0$); and the one without splitter blades at the peak efficiency point ($q_\mathrm{m}/q_\mathrm{m,PE} = 1.0$, $n/n_\mathrm{DES} = 0.8$), near choke ($q_\mathrm{m}/q_\mathrm{m,PE} = 1.2$, $n/n_\mathrm{DES} = 0.8$) and near stall ($q_\mathrm{m}/q_\mathrm{m,PE} = 0.8$, $n/n_\mathrm{DES} = 0.8$). The operating points near stall and choke were chosen by comparing the measured operating maps and typical values used in the literature. The minimum normalised near stall mass flow rate found in the literature was 0.70 [24]. The maximum normalised near stall mass flow rate was 0.91 [25]. The minimum normalised near choke mass flow rate was 1.05 [26]. The maximum normalised near choke mass flow was 1.30 [27]. The near stall point does

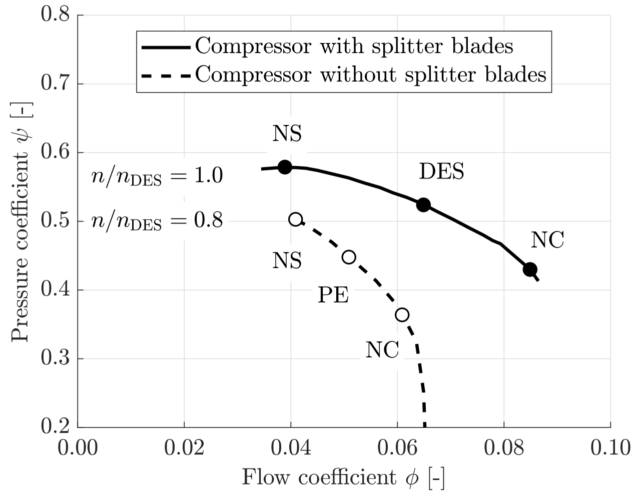

Figure 2: Dimensionless compressor map

not represent the real stall point, but is the point at a low flow rate that converges stably when modelled.

The modelled operating points are shown in Fig. 2. All the compressor performance curves were provided by Jaatinen-Värri et al. [28] for the compressor with splitter blades. For the compressor without splitter blades, the compressor performance curves were provided by Ziegler et al. [23].

In addition to three operating conditions at the baseline Reynolds number, Re_{ref}, a low Reynolds number case was also studied. Three operating conditions at the baseline Reynolds number were used to validate the numerical results against experimental data.

The Reynolds number can be varied by changing either the compressor size or the compressor inlet conditions. As demonstrated in a previous paper by the authors [19], the Reynolds number variation method does not affect the loss generation. In the present study, low Reynolds numbers were achieved by downscaling all geometric dimensions of the compressors with the same scaling factor as the impeller outlet diameter

$$SF = \frac{D_{2,\mathrm{scaled}}}{D_{2,\mathrm{baseline}}}. \tag{1}$$

Also, the same ideal gas properties of air were used for the downscaled compressors as those employed for the baseline compressor. All of the dimensionless numbers (flow coefficient ϕ, pressure coefficient ψ, and impeller tip speed Mach number Ma_{U}) were kept constant, except for the Reynolds number, which decreased as the compressor was downscaled. The studied chord Reynolds number ($Re_{\mathrm{c}} = \frac{w_1 c}{\nu_1}$) varied from 1,700,000 to 80,000, with the scaling factor varying from 1 to 0.05. The downscaled compressors were modelled at the design/peak efficiency points.

3. Numerical Model

The commercial software ANSYS CFX 17.0 was employed for the numerical calculations. The total pressure and total temperature were specified at the inlet boundary, and the mass flow rate at the outlet boundary. The computational domains are shown in Fig. 1, on which the inlet is marked with blue and the outlet with red. Turbulence was modelled using the two-equation $k-\omega$ shear stress transport (SST) model developed by Menter [29]. This model is widely used and has been validated for turbomachinery applications [30]. The values of the non-dimensional wall distance were below unity on most of the surfaces, with the most challenging region for meshing being the stagnation point at the blade leading edge.

In Fig. 3, the non-dimensional wall distance is shown in both compressors and the values above unity are clipped. The regions with the values

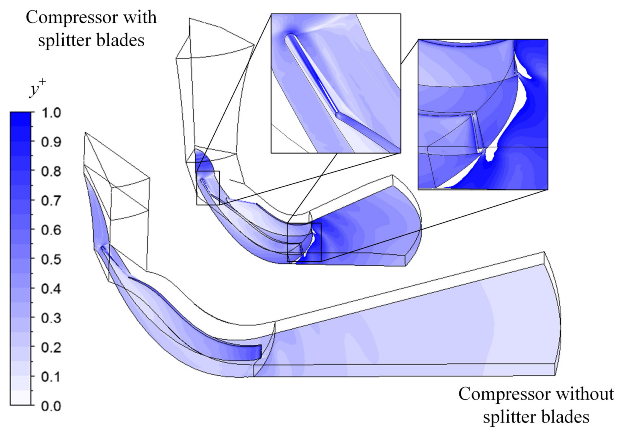

Figure 3: Values of non-dimensional wall distance (y^+) on the compressor surfaces. Values above unity are clipped and highlighted in the compressor with splitter blades.

above unity are highlighted in the compressor with splitter blades, the maximum value being 35 on the blade surface and two in the diffuser. Overall, more than ten mesh cells were located inside the boundary layer. The turbulence model was used because it switches automatically from a low-Reynolds-number treatment to wall functions if the mesh is not dense enough locally for a low-Reynolds number treatment [31], and it combines the advantages of $k-\epsilon$ and $k-\omega$ models being robust and reasonably accurate in complex flow fields as inside centrifugal compressors.

The frozen rotor approach was used to model the transition between the rotating and stationary domains. The target values for numerical convergence were the efficiency and mass imbalance between the inlet and outlet. Convergence was achieved when the change in the target values was below 0.1%, and the change in the normalised residuals of energy, mass, momentum, and turbulence parameters was stabilised.

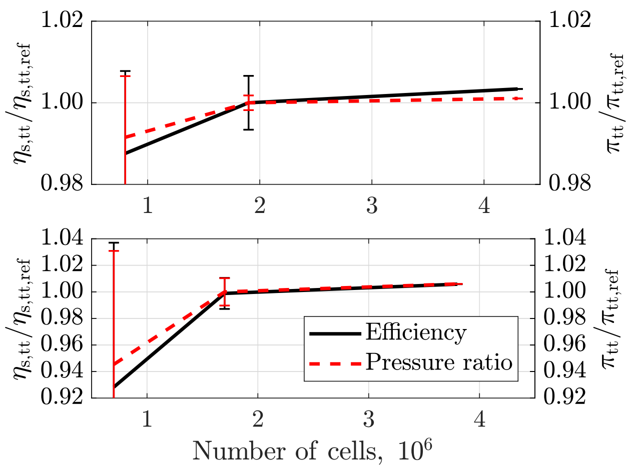

Figure 4: Mesh independence of the compressors with splitter blades (top) and without splitter blades (bottom). The ordinate is heavily scaled to show variation.

3.1. Mesh Independence Study

For the mesh independence study, three structured meshes with 0.8, 1.9, and 4.3 million computational cells were used for the compressor with splitter blades, and three meshes with 0.7, 1.7, and 3.8 million cells for the compressor without splitter blades. As a result of the mesh independence study, the meshes with 1.9 and 1.7 million cells were chosen for the compressors with and without splitter blades respectively. The target values regarding mesh independence were the total-to-total efficiency and total-to-total pressure ratio between the computational domain inlet and diffuser outlet. The discretisation error was estimated using the procedure presented by Celik et al. [32]. The estimated discretisation error is shown in Fig. 4, which presents the results of the mesh independence study for the compressors with splitter blades (top) and without splitter blades (bottom). The meshes of the baseline compressors were scaled for the downscaled compressors such that they

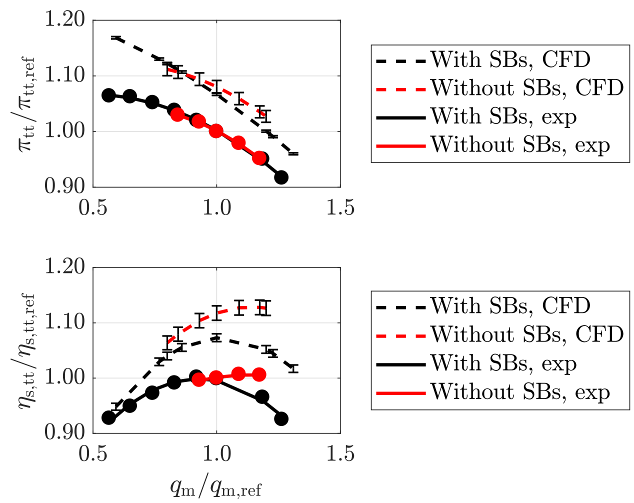

Figure 5: Validation of computational results for the pressure ratio (top) and efficiency (bottom) against the experimental data

had the same number of cells in both the baseline and the downscaled cases.

3.2. Validation Against Experimental Data

The numerical results for the baseline, non-scaled compressors were compared to the experimental results. The computational and measured total-to-total pressure ratios and efficiencies with discretisation errors are shown as functions of the normalised mass flow rate in Fig. 5. The efficiency and pressure ratio were normalised by the measured value at the design/peak efficiency point, and the mass flow rate was normalised by the design/peak efficiency mass flow rate.

The validation of the numerical model shows an over-prediction of the efficiency and pressure ratio in both cases, but still the trend is captured. It must be noted that the computational efficiency and pressure ratio were calculated between the computational domain inlet and diffuser outlet, whereas the measurements were conducted between the compressor inlet and outlet for both compressors. Therefore, the computational results do not account for the pressure loss in the volute or in the exit cone, which can be seen as part of the difference between the computational and measured values (approximately $1.5-6\%$ in the investigated compressors). The estimation is based on the total pressure loss coefficient of $0.4-0.85$ for the volute and exit cone measured by Hagelstein et al. [33], and in the compressor with splitter blades, the experimental results indicated that the volute and the exit cone were responsible for approximately 4% of the additional losses at the design point. The losses due to disk friction, leakage flow through the backside cavity, or surface roughness were also neglected in the computational model. According to Sun et al. [34], leakage through the backside cavity can be responsible for approximately 1% of additional losses in the pressure ratio and efficiency. Part of the difference between the computational and measured results was also due to the inability of the two equation models to predict all the losses.

Despite the over-prediction of the efficiency and pressure ratio, the computational model predicted the flow field fairly accurately; e.g., the relative differences between the area-averaged measured and modelled values of the absolute velocity, relative velocity and absolute flow angle (from the radial direction) in the compressor without splitter blades at $r/r_2 = 0.99$ were -2.5%, -1.7% and +1.0%, respectively (Fig. 6). A similar numerical approach to that used in this study was employed by Bareiß et al. [35], and the comparison of their numerical results against the experimental ones showed that the model overpredicted the total-to-total pressure ratio by 7.4% and the

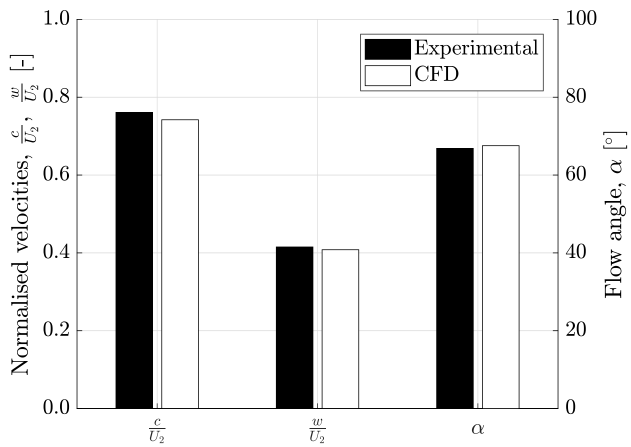

Figure 6: Validation of computational results of normalised absolute velocity, normalised relative velocity, and flow angle (from the radial direction) in the compressor without splitter blades at $r/r_2 = 0.99$ against experimental data

total-to-total isentropic efficiency by 8.9% at the design point, the values being similar to those employed in this study.

4. Correction Equations

The numerical results for the downscaled, low-Reynolds-number compressors were compared to the empirical correction equations, which are presented in Table 2. The empirical correction equations cannot replace measurements; however, because they are based on experimental data, they represent an acceptable alternative to experiments and can be used to validate the trends of the numerical results. To validate the numerical results in full detail, experimental data of the flow fields inside a low-Reynolds-number compressor should be available for comparison to the flow fields inside a high-Reynolds-number compressor.

Table 2: Summary of the efficiency correction equations published in the literature

Reference	Equation	
Old empirical formula [36]	$\frac{1-\eta}{1-\eta_{\mathrm{ref}}} = a + (1-a)\left[\frac{Re_{\mathrm{ref}}}{Re}\right]^n$	(2)
Casey (1985) [37]	$\Delta\eta = -\frac{c}{\mu_0}\Delta f$	(3)
Heß & Pelz (2010) [38]	$\frac{1-\eta}{1-\eta_{\mathrm{ref}}} = (1-b) + b\left(\frac{Re_{\mathrm{ref}}}{Re}\right)^n$	(4)
Casey & Robinson (2011) [7]	$\Delta\eta = -\frac{B_{\mathrm{ref}}}{f_{\mathrm{ref}}}\Delta f$	(5)
Dietmann & Casey (2013) [20]	$\Delta\eta = -\frac{B_{\mathrm{ref}}}{f_{\mathrm{ref}}}\Delta f$	(6)
Pelz & Stonjek (2013) [39]	$\Delta\eta = -\frac{1-\eta_{\mathrm{ref}}}{c_{\mathrm{f,ref}}}\Delta c_{\mathrm{f}}$	(7)

The results in Fig. 7 indicate that the compressor's total-to-total isentropic efficiency decreased as the Reynolds number decreased, as predicted by the correction equation published by Dietmann and Casey [20]. According to Eqn. (6), which was provided by Dietmann and Casey [20], a change in the Reynolds number causes a change in the friction factor, which results in a change in the efficiency. The term B_{ref} refers to inefficiency due to friction losses, while f_{ref} refers to the friction factor at the reference conditions. The term B_{ref} is based on experimental data from over 30 compressors ($Re_{\mathrm{c}} = 50,000 \ldots 100,000,000$), and depends on the flow coefficient as follows:

$$B_{\mathrm{ref}} = 0.05 + \frac{0.002}{\phi + 0.0025}. \tag{8}$$

5. Results

The results are shown for the baseline compressor at the design/peak efficiency point (DES/PE), near stall (NS) and near choke (NC) conditions and

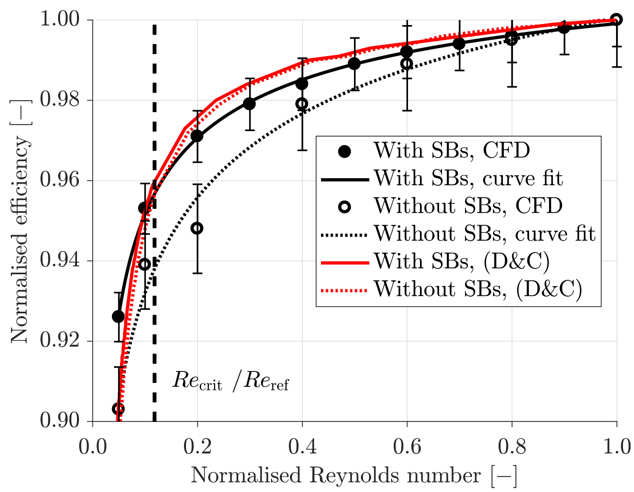

Figure 7: Change in total-to-total isentropic efficiency with a varying Reynolds number

for the smallest downscaled compressor (SF=0.05) at the design/peak efficiency point. The impeller outlet diameter of the smallest downscaled compressor (16.6 mm with splitter blades and 13.5 mm without splitter blades) is of the same order of magnitude as that of the centrifugal compressor manufactured by Isomura et al. [40] (10 mm). Additionally, a small-scale compressor (12 mm) was manufactured by Kang et al. [41]. In this study, the manufacturing tolerances of the blade thickness or tip clearance were not accounted for in order to purely investigate the Reynolds number losses.

The preliminary results presented previously by the authors [18] showed that the largest fraction of the losses was generated in the tip clearance and blade boundary layers of the compressor with splitter blades. However, the analysis suffered due to the difficulty calculating the boundary layer thickness inside the blade passage of a centrifugal compressor. The previous results by the authors [21] showed that the constantly increasing boundary layer thickness of a flat plate has its weaknesses in the case of a centrifugal compressor due to the jet-wake flow structure and locally increasing relative velocity. Thus, the authors proposed a hybrid method for calculating the boundary layer thickness inside a complex centrifugal compressor flow field [21]. This approach was employed in this study because it made it possible to analyse loss generation with a more sophisticated approach.

When the hybrid method is employed, the velocity profile on the line perpendicular to the investigated surface is exported for the post-processing purposes. The number of lines in the meridional direction is specified by the user. Firstly, the flow is assumed attached, and the free-stream velocity and boundary layer thickness are calculated as follows:

$$\frac{dU}{dn} = 0.005 \Rightarrow U_{\mathrm{n}-1} = 0.995 U_{\mathrm{n}}. \tag{9}$$

Hence, the boundary layer thickness is the distance between the surface and the location where the velocity is 99.5% of the velocity of the adjacent data point. Secondly, the average value of for the free-stream velocities in the meridional direction is calculated as follows:

$$U_{\infty,\mathrm{ave}} = \frac{1}{N}\sum_{1}^{N} U_{\mathrm{n}}. \tag{10}$$

Thirdly, the velocity profile is plotted and flow separation on the blade suction side near the leading edge is qualitatively analysed from the plot by the user. Fourthly, the locations of flow separation are specified by the user. Finally, the free-stream velocity and boundary layer thickness are calculated for attached flow by using Eqn. (9) and for separated flow, as follows:

$$U_{\delta} = 0.995 U_{\infty,\mathrm{ave}}. \tag{11}$$

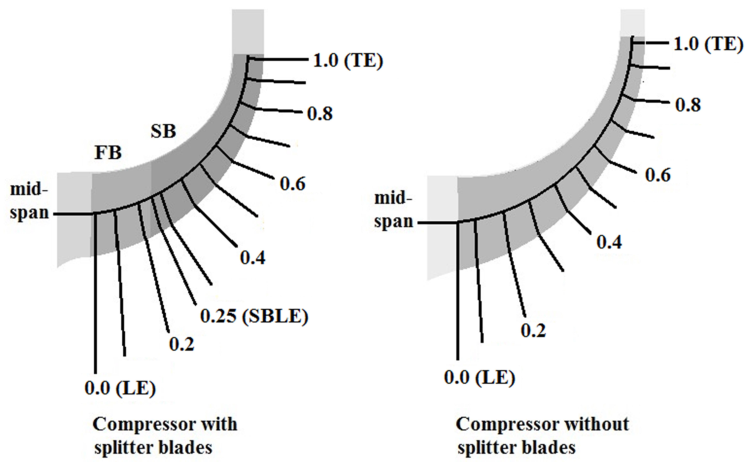

Figure 8: Observation planes along the meridional direction from the full blade (FB) leading edge (LE) to the trailing edge (TE)

5.1. Boundary Layer Losses at the Blade Surfaces

The hybrid method described above was used to calculate the blade boundary layer thickness. The observation planes in the meridional direction are shown in Fig. 8. Figures 9 and 10 provide a sum of the boundary layer thickness near the blade surfaces ($\delta_{\mathrm{FBPS}} + \delta_{\mathrm{FBSS}} + \delta_{\mathrm{SBPS}} + \delta_{\mathrm{SBSS}}$) from the blade leading edge (0.0) to the trailing edge (1.0) in the compressors without and with splitter blades respectively. The boundary layer thickness was normalised by the pitchwise length of the modelled compressor blade passage at the impeller outlet. Based on the sensitivity analysis [21], the relative velocity values of 10,000 data points in the pitchwise direction were analysed. The data points were located at the mid-span in order to exclude the effect of the endwall boundary layers on the blade boundary layers.

The results in Figs. 9 and 10 indicate no change in the boundary layer

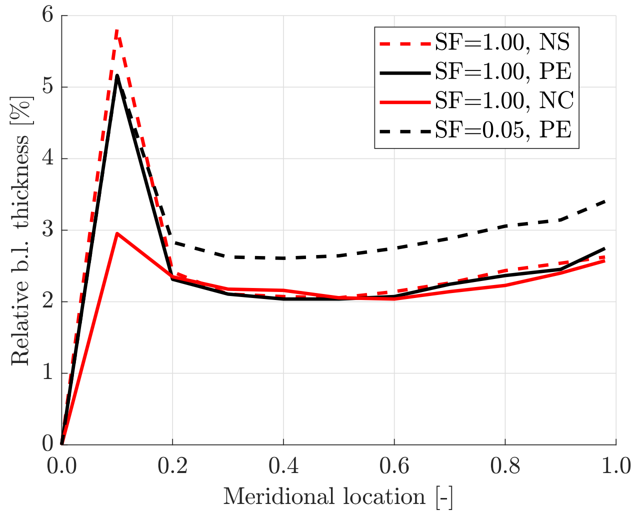

Figure 9: Sum of the relative boundary layer thickness near the full blade pressure and suction surfaces ($\delta_{\text{FBPS}} + \delta_{\text{FBSS}}$) in the compressor without splitter blades

thickness under different operating conditions at a high Reynolds number (SF=1.00), except for a separation point at 10% chord length from the leading edge. However, the boundary layer thickness increased, on average, by 30 and 36% at a low Reynolds number (SF=0.05) in the compressors without and with splitter blades, respectively. In the compressor with splitter blades (Fig. 9), the summarised boundary layer thickness increased downstream to the separation point due to the increased boundary layer thickness around the splitter blade (the splitter blade leading edge at a meridional location of 0.25); this stands in contrast to the other compressor. Table 3 shows how the boundary layer thickness, averaged over the blade length, changed in the near-stall, near-choke and low-Reynolds-number cases compared to the baseline case (SF=1.00, DES); the change was insignificant under the off-design conditions, but remarkable in the low-Reynolds-number case.

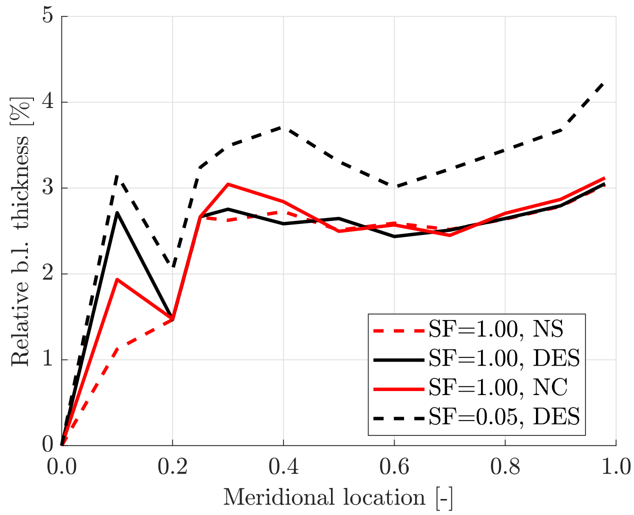

Figure 10: Sum of the relative boundary layer thickness near the full and splitter blade pressure and suction surfaces ($\delta_{\mathrm{FBPS}} + \delta_{\mathrm{FBSS}} + \delta_{\mathrm{SBPS}} + \delta_{\mathrm{SBSS}}$) in the compressor with splitter blades

Table 3: Relative increase in the average blade boundary layer thickness in the blade passage compared to the baseline case at the design/peak efficiency point (SF=1.00, DES/PE)

	SF=1.00, NS	SF=1.00, NC	SF=0.05, DES/PE
Without splitter blades	+3%	−5%	+30%
With splitter blades	−5%	±0%	+36%

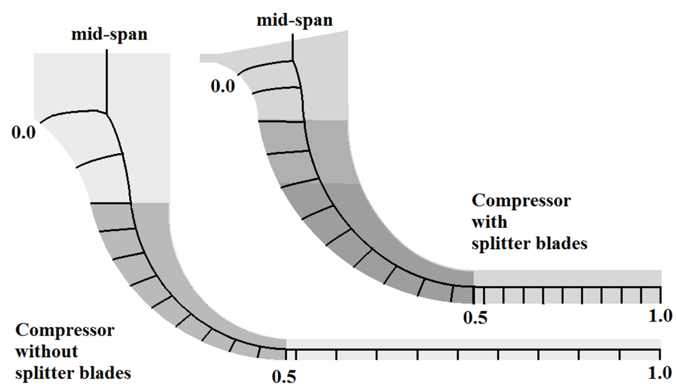

Figure 11: Observation locations in the meridional direction from the impeller inlet (0.0) to the diffuser outlet (1.0)

5.2. Boundary Layer Losses at the Endwalls

When calculating the boundary layer thickness at the impeller and diffuser endwalls, the relative and absolute velocities, respectively were analysed. In total, 22 locations in the meridional direction from the impeller inlet (0.0) to the diffuser outlet (1.0) were investigated. The observation locations in the meridional direction are shown in Fig. 11. The velocity was averaged in the pitchwise direction based on ten investigated locations, and the boundary layer thickness from the spanwise distribution was calculated. The method was less sensitive to the number of data points in the spanwise direction than in the pitchwise direction. For this reason, based on the sensitivity analysis, in this study, 160 points were analysed in the impeller and 100 points in the diffuser.

Increased boundary layer thickness was clearly visible near the diffuser hub and diffuser shroud of the investigated compressors (Figs. 12 and 13). In the compressor without splitter blades (Fig. 12), the maximum thickness of

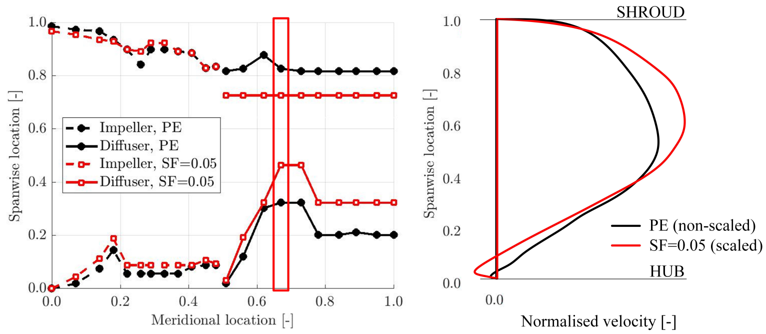

Figure 12: Left: Boundary layer thickness normalised by the passage height near the hub ($b/b_{\text{shroud}} = 0.0$) and shroud ($b/b_{\text{shroud}} = 1.0$) in the compressor without splitter blades. Right: Velocity profile projected in the radial direction at the meridional location, marked with a red rectangle.

the boundary layer near the diffuser hub was located at a meridional location of 0.67 ($r/r_2 = 1.52$, marked with a red rectangle) as a result of reverse flow. The velocity profile on the right-hand side in Fig. 12 illustrates the reverse flow near the hub.

In the compressor with splitter blades (Fig. 13), the boundary layer thickness increased near the hub and shroud from the impeller inlet to the diffuser outlet. In the low-Reynolds-number compressor (SF=0.05), the reversed flow near the hub at the diffuser outlet led to an increase of 200% in the boundary layer thickness compared to the baseline compressor (DES). The reverse flow is illustrated by the velocity profile on the right-hand side in Fig. 13.

Table 4 presents the relative increase in the average endwall boundary layer thicknesses in the smallest downscaled compressor compared to the baseline case at the design/peak efficiency point. The comparison of the results in Tables 3 and 4 indicates greater thickening of the boundary layer, on

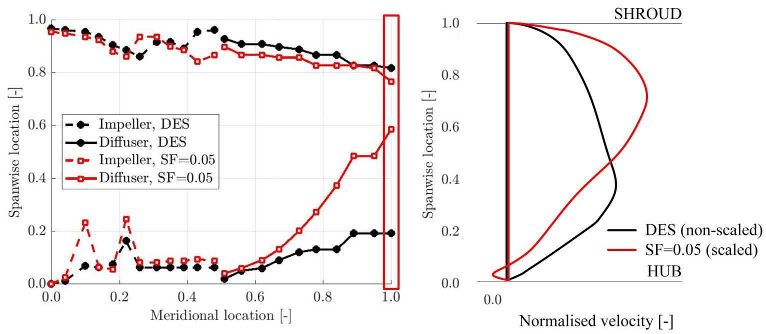

Figure 13: Left: Boundary layer thickness normalised by the passage height near the hub ($b/b_{\mathrm{shroud}} = 0.0$) and shroud ($b/b_{\mathrm{shroud}} = 1.0$) in the compressor with splitter blades. Right: Velocity profile projected in the radial direction at the meridional location, marked with a red rectangle.

Table 4: Relative increase on the average endwall boundary layer thicknesses in the smallest downscaled compressor (SF=0.05, DES/PE) compared to the baseline case at the design/peak efficiency point (SF=1.00, DES/PE)

	With splitter blades	Without splitter blades
Endwall average	+62%	+45%
Impeller average	+54%	+35%
Impeller shroud	+54%	+21%
Impeller hub	+54%	+48%
Diffuser average	+69%	+55%
Diffuser shroud	+29%	+59%
Diffuser hub	+108%	+50%

average, near the endwalls than near the blade surfaces. In both compressors, the boundary layer thickness increased more, on average, in the diffuser than in the impeller. The greater thickening of the boundary layer near the impeller hub than that near the blade surfaces might result from the secondary flow, which shifts the low-momentum fluid towards the impeller hub and further along the blade surfaces to the wake located in the shroud suction side corner- of the blade passage [42]. In the diffuser, the low-momentum fluid from the boundary layers is not shifted to the wake as it is in the impeller, resulting in greater thickening of the boundary layers.

More detailed investigation of the relative increase in the boundary layer thickness indicated that the endwall boundary layer thickness increased more at the impeller hub than at the impeller shroud in the compressor without splitter blades, whereas in the compressor with splitter blades, the increase was equal at the impeller hub and shroud. The greater increase of the impeller shroud boundary layer thickness in the compressor with splitter blades might be due to the larger relative tip clearance than in the compressor without splitter blades.

The relatively thicker boundary layers result in increased blockage, which is observed as increased radial velocity. The velocity profiles on the right-hand side of Figs. 12 and 13 indicate increased velocity due to the increased blockage and Table 5 shows the average increase in the radial velocity at the diffuser inlet and outlet in the low-Reynolds-number case compared to the baseline case. The radial velocity is calculated from the mass flow rate through the computational domain, pitchwise-averaged density distribution from the numerical simulation, and cross-sectional area of the computational

Table 5: Relative change in the radial velocity component at the diffuser inlet ($r/r_2 = 1.04$) and outlet (r_3) compared to the baseline case at the design/peak efficiency point (SF=1.00, DES/PE)

		SF=0.05, DES/PE
Without splitter blades	Diffuser inlet, $r/r_2 = 1.04$	+7.1%
Without splitter blades	Diffuser outlet, $r_3/r_2 = 2.48$	+8.6%
With splitter blades	Diffuser inlet, $r/r_2 = 1.04$	+5.1%
With splitter blades	Diffuser outlet, $r_3/r_2 = 1.68$	+5.2%

domain as follows:

$$c_{\mathrm{r}} = \frac{q_{\mathrm{m,domain}}}{\rho A_{\mathrm{domain}}}. \tag{12}$$

The normalised radial velocity is averaged in the spanwise direction in order to calculate the relative increase. The increased radial velocity increases the wall shear stress and decreases the static pressure, resulting in greater friction losses and weaker compressor performance. The results presented in this subsection indicate that the method that exhibits the most potential to decrease the losses due to low Reynolds numbers involves controlling the boundary layers near the impeller hub and diffuser surfaces. The result of the diffuser's significant role in the performance deterioration is in contrast to previous knowledge; i.e., most of the losses occur in the impeller due to the high flow velocities [20].

5.3. Losses Associated with Tip Clearance

The losses associated with the tip clearance are difficult to distinguish from the boundary layer losses near the impeller shroud due to the tip leakage flow. However, in many compressors, the blade boundary layer, endwall

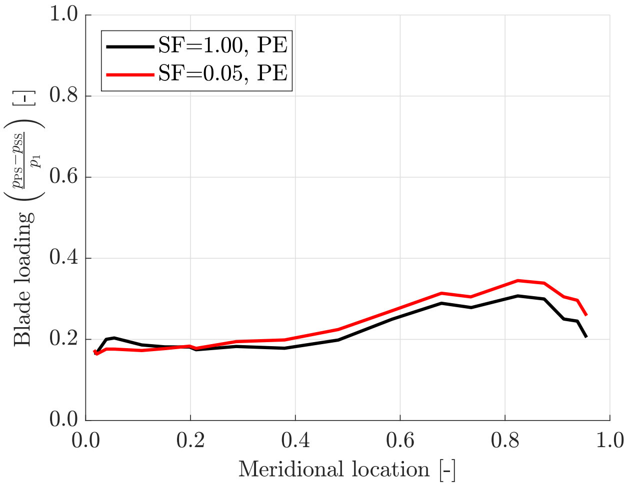

Figure 14: Blade loading defined as a normalised pressure difference across the blade at the 95% span of the compressor without splitter blades

boundary layer and tip leakage losses are of the same order of magnitude [43]. To analyse the effect of the decreased Reynolds number on the tip leakage losses, the blade loading is investigated. In Fig. 14, the blade loading at the 95% span is defined as a pressure difference across the blade normalised by the pressure at the compressor inlet. The blade loading increased by 7% on average in the smallest downscaled compressor compared to the baseline case. As the pressure difference across the blade drives the tip leakage flow from the pressure side to the suction side and the increased blade loading corresponds to the strengthened tip leakage flow [44], the results presented in Fig. 14 indicate that the tip leakage strengthened with the decreased Reynolds number when the relative tip clearance remained constant.

However, in micro-scale centrifugal compressors, the relatively larger tip clearances due to the manufacturing and controlling reasons would result in further increased tip leakage losses. The numerical results of this work indicated that a 100% larger relative tip clearance (from 25 μm to 50 μm) in the smallest downscaled compressor without splitter blades resulted in a less than 1% additional decrease in the efficiency. This result agrees with the results presented elsewhere [45].

5.4. Overall Losses

The increased friction losses of the low-Reynolds-number compressor result in an increased total pressure loss coefficient:

$$K_{\mathrm{p}} = \frac{p_{\mathrm{t},2} - p_{\mathrm{t},3}}{p_{\mathrm{t},2} - p_{\mathrm{s},2}}, \tag{13}$$

which is presented in Fig. 15 as a function of the Reynolds number for both compressors. At the critical chord Reynolds number (200,000), the increase in the total pressure loss was approximately 40% in the compressor without splitter blades and 30% in the compressor with splitter blades.

Additionally, Figure 16 presents the pressure recovery coefficient

$$C_{\mathrm{pr}} = \frac{p_{\mathrm{s},3} - p_{\mathrm{s},2}}{p_{\mathrm{t},2} - p_{\mathrm{s},2}} \tag{14}$$

as a function of the Reynolds number. At the critical chord Reynolds number, the decrease in the pressure recovery coefficient was approximately 10% for both compressors. Figure 17 shows both the impeller and compressor stage efficiencies, which were calculated using Eqns. (15) and (16), respectively, and based on the adiabatic assumption, $T_{\mathrm{t2}} = T_{\mathrm{t3}}$.

$$\eta_{\mathrm{s,t1-t2}} = \frac{\left(\frac{p_{\mathrm{t2}}}{p_{\mathrm{t1}}}\right)^{\frac{R}{c_{\mathrm{p}}}} - 1}{\frac{T_{\mathrm{t2}}}{T_{\mathrm{t1}}} - 1} \tag{15}$$

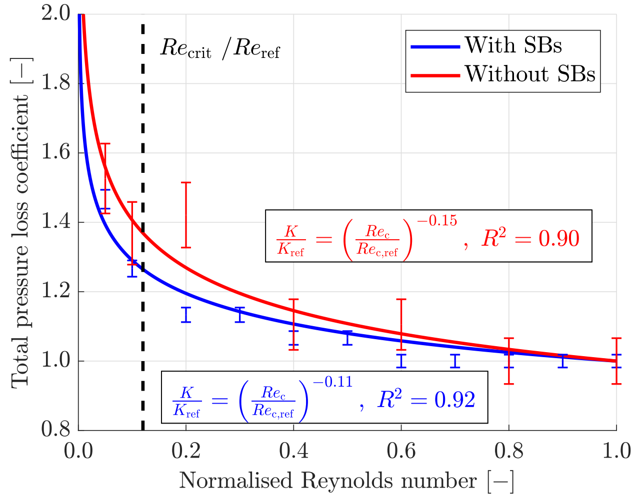

Figure 15: Change in a normalised total pressure loss coefficient with a varying Reynolds number. $R^2 = 0.92$ with splitter blades (SBs) and $R^2 = 0.90$ without splitter blades.

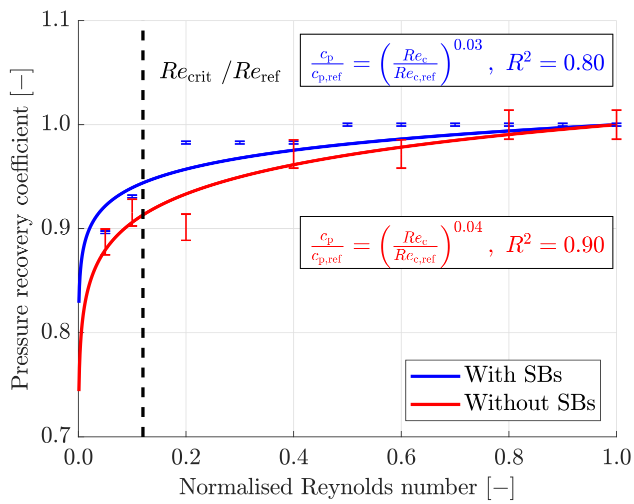

Figure 16: Change in a normalised pressure recovery coefficient with a varying Reynolds number. $R^2 = 0.80$ with splitter blades (SBs) and $R^2 = 0.90$ without splitter blades.

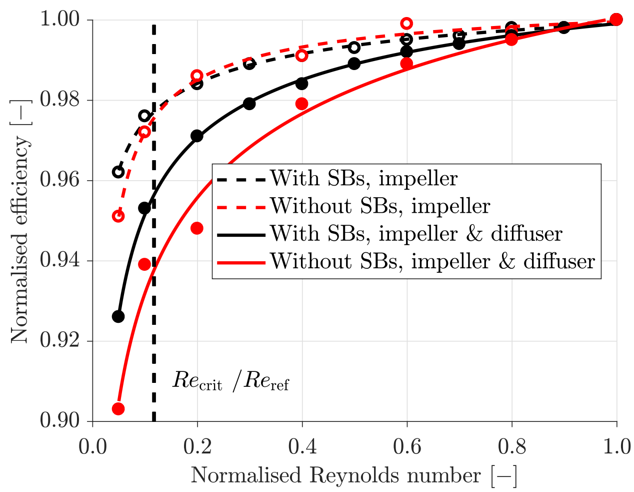

Figure 17: Change in impeller efficiency (dash line) and compressor stage efficiency (solid line) with a varying Reynolds number

$$\eta_{\mathrm{s,t1-t3}} = \frac{\left(\frac{p_{\mathrm{t3}}}{p_{\mathrm{t1}}}\right)^{\frac{R}{\bar{c}_{\mathrm{p}}}} - 1}{\frac{T_{\mathrm{t3}}}{T_{\mathrm{t1}}} - 1} \tag{16}$$

The results shown in Figs. 15 − 17 indicate that the diffuser had a significant influence on the performance deterioration of the low-Reynolds-number compressors. When the Reynolds number decreased by 90% (from the baseline to the critical Reynolds number), the impeller caused 54% and the diffuser 46% of the efficiency deterioration in the compressor with splitter blades. In the compressor without splitter blades, the respective values were 50% (impeller) and 50% (diffuser). And, as shown in Table 4, the boundary layer growth was greater near the diffuser endwalls than near the impeller endwalls. The calculation of the changes in the mass-flow-averaged specific entropy of the impeller and diffuser strengthens this argument; e.g., in the compressor with splitter blades at the baseline Reynolds number, 58% of the total specific entropy increase occurred in the impeller and 42% in the diffuser, whereas in the smallest downscaled compressor, the fraction of the diffuser increased to 47%. In the compressor without splitter blades, 36% of the total specific entropy increase occurred in the diffuser at the baseline Reynolds number, and 46% at the lowest investigated Reynolds number (in the smallest downscaled compressor). These results indicate that the role of the diffuser on the performance deterioration strengthens with the decreasing Reynolds number. Therefore, the diffuser should be included in the loss development analysis even though recent investigations have mainly focused on the impeller.

The deterioration in performance observed as the decreased efficiency in the present study exhibited a similar trend (Fig. 7) as predicted by the correction equation of Dietmann and Casey [20]. In the present study, the fully turbulent flow field was assumed, and the transition from laminar to turbulent flow was not accounted for. However, it is not obvious whether the transition model should be used or not when modelling the low-Reynolds-number flows in centrifugal compressors. Previously, different approaches have been employed to model small-scale centrifugal compressors. For example, the standard $k-\epsilon$ model [46], Chien's low-Reynolds-number $k-\epsilon$ model [41], a model proposed by Spalart and Allmaras [47] and even a laminar approach [48]. In the present study, the influence of transition on turbulence modelling was investigated using the SST $k-\omega$ model in combination with the $\gamma - Re_\theta$ transition model proposed by Langtry and Menter [49]. According to the results of this study, accounting for the transition did not change the results from the fully turbulent solution. The transition model could capture the laminar separation; however, because the flow separation near the blade leading edge resulted from the centrifugal force and not from the laminar separation, the modelling of transition in the centrifugal compressor did not add value.

Since the efficiency correction equation proposed by Dietmann and Casey [20] is based on the experimental data of over 30 compressors, the numerical results in this study were compared to their experimental data. Simply measuring a micro-scale compressor would not have yielded original results because there is already data available on low-Reynolds-number compressors [20]. In addition, experimental data of micro-scale compressors exists [41]. While information about the flow field inside the micro-scale compressor would introduce a certain degree of novelty, as long as the lack of micro-scale measurement instruments continue to limit the experiments, the flow fields still needs to be studied with the help of computational fluid dynamics.

The results presented above provide an overview of the loss generation due to low Reynolds numbers.

6. Discussion

Is there a way to counter the reduction in efficiency of a compressor that is caused by the low Reynolds number? Based on the numerical results, the increased boundary layer thickness most strongly affects the diminished efficiency in the low-Reynolds-number compressors. Therefore, the efficiency could be increased by controlling the boundary layer. Controlling the impeller hub and diffuser boundary layers would result in the most significant reduction in losses.

To decrease the boundary layer thickness, the low-momentum fluid near the surface should be either accelerated or removed. The difficulties in using the boundary layer acceleration or suction inside a centrifugal compressor stem from the requirement for pressurised air and a control device. The flow from the blade pressure side to the suction side through small holes could accelerate the boundary layer flow on the blade suction side, but the holes would decrease the mechanical strength and loading. The boundary layer control would be easier on the stationary diffuser endwalls, but implementing the control device would be challenging, especially in the case of micro-scale, low-Reynolds-number compressors; their advantages include added savings in size and weight.

In a vaned diffuser, researchers have proved that a sufficiently simple flow control method called the porous throat diffuser, which links the throats of the diffuser passages via a side cavity, broadens the operating range due to a more uniform pressure distribution [50]. The applicability of this kind of simple configuration for a vaneless diffuser should be investigated in the future. To conclude, the improvement in the low-Reynolds-number compressor's performance would require an innovative means for boundary layer control without the need for external control devices.

7. Conclusions

At a low Reynolds number:

- Blade boundary layer thickness increases, on average, from approximately 30% to 36%;

- Endwall boundary layer thickness increases, on average, from approximately 45% to 62%;

- Tip leakage strengthens;

- Blockage due to thicker boundary layers increases the radial velocity component at the diffuser outlet from 5% to 9%. The increased radial velocity increases the wall shear stress and decreases the static pressure;

- The 90% decrease in the Reynolds number results in a $30-40\%$ increase in the total pressure loss coefficient and in a 10% reduction in the pressure recovery coefficient;

- The impeller accounts for $50-54\%$ and the diffuser $46-50\%$ of the efficiency deterioration, and the role of the diffuser in the performance deterioration strengthens with the decreasing Reynolds number;

- The 100% increase in the relative tip clearance (from 0.045 to 0.091) results in an additional 1% reduction in efficiency;

- Modelling transition in the centrifugal compressor does not add value compared to the computational cost of the process, as the flow separates near the leading edge due to centrifugal force, regardless of whether or not the laminar separation occurs.

To improve the performance of the centrifugal compressors that operate at low Reynolds numbers, the boundary layers near the impeller hub, and especially in the diffuser, should be suppressed. However, the use of control devices for boundary layer acceleration or suction is problematic because their small size and low weight make micro-scale gas turbines the more attractive alternative to batteries and piston engine-based power modules; however, the control devices required for these would increase the overall weight of the compressors.

Future work should focus on the development of an innovative means of boundary layer control without the need for external control devices in order to improve the low-Reynolds-number compressor's performance.

Acknowledgements

The authors would like to thank Michael Casey for the suggestion to study the influence of transitional turbulence modelling and would also like to acknowledge the financial contribution of the Academy of Finland. This research is part of the "Low-Reynolds number kinetic compression" project, which was funded by the Academy of Finland under grant number 274897.

References

[1] the United Nations, [In the United Nations www-pages]. [retrieved December 15, 2017]. From: http://www.un.org/sustainabledevelopment (2015).

[2] the European Commission, [In the European Commission www-pages]. [retrieved December 18, 2017]. From: https://ec.europa.eu/energy/en/topics/energy-strategy-and-energy-union/2050-energy-strategy (2012).

[3] the Parliamentary Committee on Energy, C. Issues, Energy and Climate Roadmap 2050 – Report of the Parliamentary Committee on Energy and Climate Issues on 16 October 2014, Publications of the Ministry of Employment and the Economy. Energy and the climate 50/2014. ISBN 978-952-227-906-4, p. 77 (2014).

[4] D. Vittorini, R. Cipollone, Energy Saving Potential in Existing Industrial Compressors, Energy 102 (2016) 502 – 515. doi:10.1016/j.energy.2016.02.115.

[5] the International Energy Agency, [In the International Energy Agency www-pages]. [retrieved January 3, 2018]. From: http://www.iea.org/publications/freepublications/publication/Energy_Efficiency_2017.pdf (2017).

[6] M. Casey, D. Krähenbuhl, C. Zwyssig, The Design of Ultra-High-Speed Miniature Centrifugal Compressors, in: J. Backman, G. Bois, O. Leonard (Eds.), Proceedings of the 10th European Conference on Turbomachinery: Fluid Dynamics and Thermodynamics, 2013, pp. 506 – 519, April 15-19, 2013, Lappeenranta, Finland.

[7] M. Casey, C. Robinson, A Unified Correction Method for Reynolds Number, Size, and Roughness Effects on the Performance of Compressors, Proceedings of the Institution of Mechanical Engineers, Part A: Journal of Power and Energy 225 (7) (2011) 864–876. doi:10.1177/0957650911410161.

[8] S. Yang, S. Chen, X. Chen, X. Zhang, Y. Hou, Study on

the Coupling Performance of a Turboexpander Compressor Applied in Cryogenic Reverse Brayton Air Refrigerator, Energy Conversion and Management 122 (2016) 386 – 399. doi:http://dx.doi.org/10.1016/j.enconman.2016.05.092.

[9] S. Martinez, G. Michaux, P. Salagnac, J.-L. Bouvier, Micro-Combined Heat and Power Systems (Micro-CHP) Based on Renewable Energy Sources, Energy Conversion and Management 154 (Supplement C) (2017) 262 – 285. doi:10.1016/j.enconman.2017.10.035.

[10] J. Backman, J. Kaikko, Microturbine Systems for Small Combined Heat and Power (CHP) Applications, in: R. Beith (Ed.), Small and Micro Combined Heat and Power (CHP) Systems, Woodhead Publishing Series in Energy, Woodhead Publishing, 2011, Ch. 7, pp. 147–178. doi:10.1533/9780857092755.2.147.

[11] W. Visser, S. Shakariyants, M. De Later, A. Haj Ayed, K. Kusterer, Performance Optimization of a 3kW Microturbine for CHP Applications, in: Proceedings of ASME Turbo Expo 2012: Turbine Technical Conference and Exposition, Vol. 5, 2012, pp. 619–628, paper No. GT2012-68686. June 11-15, 2012, Copenhagen, Denmark. doi:10.1115/GT2012-68686.

[12] A. Durante, G. Pena-Vergara, P. Curto-Risso, A. Medina, A. C. Hernández, Thermodynamic Simulation of a Multi-Step Externally Fired Gas Turbine Powered by Biomass, Energy Conversion and Management 140 (2017) 182 – 191. doi:10.1016/j.enconman.2017.02.050.

[13] A. Marcellan, W. Visser, P. Colonna, Potential of Micro Turbine Based

Propulsion Systems for Civil UAVs: A Case Study, in: Proceedings of the ASME Turbo Expo: Turbomachinery Technical Conference and Exposition, 2016, Paper No. GT2016-57719, p. 10. June 13 – 17, 2016, Seoul, South Korea. doi:10.1115/GT2016-57719.

[14] P. Röyttä, T. Turunen-Saaresti, J. Honkatukia, Optimising the Refrigeration Cycle with a Two-Stage Centrifugal Compressor and a Flash Intercooler, International Journal of Refrigeration 32 (6) (2009) 1366–1375. doi:10.1016/j.ijrefrig.2009.01.006.

[15] M. Schleer, R. S. Abhari, Influence of Geometric Scaling on the Stability and Range of a Turbocharger Centrifugal Compressor, in: Proceedings of ASME Turbo Expo 2005: Power for Land, Sea, and Air, 2005, pp. 859–869, Paper No. GT2005-68713. June 6–9, 2005, Reno, Nevada, USA. doi:10.1115/GT2005-68713.

[16] X. Zheng, Y. Lin, B. Gan, W. Zhuge, Y. Zhang, Effects of Reynolds Number on the Performance of a High Pressure-Ratio Turbocharger Compressor, Science China: Technological Sciences 56 (6) (2013) 1361–1369. doi:10.1007/s11431-013-5213-6.

[17] M. Choi, J. H. Baek, H. T. Chung, S. H. Oh, H. Y. Ko, Effects of the Low Reynolds Number on the Loss Characteristics in an Axial Compressor, Proceedings of the Institution of Mechanical Engineers, Part A: Journal of Power and Energy 222 (2008) 209–218. doi:10.1243/09576509JPE520.

[18] J. Tiainen, A. Jaatinen-Värri, A. Grönman, J. Backman, Numerical Study of the Reynolds Number Effect on the Centrifugal Compres-

sor Performance and Losses, in: Proceedings of the ASME Turbo Expo 2016: Turbine Technical Conference and Exposition, 2016, Paper No. GT2016-56036, p. 10. June 13 – 17, 2016, Seoul, South Korea. doi:10.1115/GT2016-56036.

[19] J. Tiainen, A. Jaatinen-Värri, A. Grönman, J. Backman, Influence of Reynolds Number Variation Method on Centrifugal Compressor Loss Generation, in: Proceedings of 12th European Conference on Turbomachinery Fluid dynamics & Thermodynamics, 2017, Paper ID: ETC2017-041, 12 pages. April 3–7, 2017, Stockholm, Sweden.

[20] F. Dietmann, M. Casey, The Effects of Reynolds Number and Roughness on Compressor Performance, in: J. Backman, G. Bois, O. Leonard (Eds.), Proceedings of the 10th European Conference on Turbomachinery: Fluid Dynamics and Thermodynamics, 2013, pp. 532 – 542, April 15–19, 2013, Lappeenranta, Finland.

[21] J. Tiainen, A. Jaatinen-Värri, A. Grönman, T. Turunen-Saaresti, J. Backman, Effect of Free-Stream Velocity Definition on Boundary Layer Thickness and Losses in Centrifugal Compressors, in: Proceedings of the ASME Turbo Expo 2017: Turbomachinery Technical Conference and Exposition, 2017, Paper No. GT2017-63268, 14 pages. June 26–30, 2017, Charlotte, NC, USA. doi:10.1115/GT2017-63268.

[22] A. Jaatinen-Värri, T. Turunen-Saaresti, P. Röyttä, A. Grönman, J. Backman, Experimental Study of Centrifugal Compressor Tip Clearance and Vaneless Diffuser Flow Fields, Proceedings of the Institution

of Mechanical Engineers, Part A: Journal of Power and Energy 227 (8) (2013) 885–895. doi:10.1177/0957650913497358.

[23] K. Ziegler, H. Gallus, R. Niehuis, A Study on Impeller-Diffuser Interaction - Part I: Influence on the Performance, Journal of Turbomachinery 125 (1) (2003) 173–182. doi:10.1115/1.1516814.

[24] A. Weber, C. Morsbach, E. Kügeler, C. Rube, M. Wedeking, Flow Analysis of a High Flowrate Centrifugal Compressor Stage and Comparison With Test Rig Data, in: Proceedings of ASME Turbo Expo 2016: Turbomachinery Technical Conference and Exposition, Vol. 2D-2016, 2016, Paper No. GT2016-56551, 12 pages. June 13–17, 2016, Seoul, South Korea. doi:10.1115/GT2016-56561.

[25] Y. Bousquet, X. Carbonneau, I. Trébinjac, G. Dufour, M. Roumeas, Description of the Unsteady Flow Pattern from Peak Efficiency to Near Surge in a Subsonic Centrifugal Compressor Stage, in: J. Backman, G. Bois, O. Leonard (Eds.), Proceedings of the 10th European Conference on Turbomachinery: Fluid Dynamics and Thermodynamics, 2013, pp. 917–927, april 15-19, 2013, Lappeenranta, Finland.

[26] M. Yang, X. Zheng, Y. Zhang, T. Bamba, H. Tamaki, J. Huenteler, Z. Li, Stability Improvement of High-Pressure-Ratio Turbocharger Centrifugal Compressor by Asymmetric Flow Control-Part I: Non-Axisymmetrical Flow in Centrifugal Compressor, Journal of Turbomachinery 135 (2) (2012) Article ID 021006, 9 pages. doi:10.1115/1.4006636.

[27] W. Xu, T. Wang, C. Gu, L. Ding, A Study on the Influence of Hole's

Diameter With Holed Casing Treatment, in: Proceedings of ASME Turbo Expo 2011, Vol. 4, 2011, pp. 499–508, Paper No. GT2011-46167, 10 pages. June 6–10, 2011, Vancouver, British Columbia, Canada. doi:10.1115/GT2011-46167.

[28] A. Jaatinen-Värri, T. Turunen-Saaresti, A. Grönman, P. Röyttä, J. Backman, The Tip Clearance Effects on the Centrifugal Compressor Vaneless Diffuser Flow Fields at Off-Design Conditions, in: J. Backman, G. Bois, O. Leonard (Eds.), Proceedings of the 10th European Conference on Turbomachinery: Fluid Dynamics and Thermodynamics, 2013, pp. 972–982, April 15-19, 2013, Lappeenranta, Finland.

[29] F. Menter, Two-Equation Eddy-Viscosity Turbulence Models for Engineering Applications, AIAA Journal 32 (8) (1994) 1598–1605. doi:10.2514/3.12149.

[30] F. Menter, Review of the Shear-Stress Transport Turbulence Model Experience from an Industrial Perspective, International Journal of Computational Fluid Dynamics 23 (4) (2009) 305–316. doi:10.1080/10618560902773387.

[31] F. Menter, J. Carregal Ferreira, T. Esch, B. Konno, The SST Turbulence Model with Improved Wall Treatment for Heat Transfer Predictions in Gas Turbines, in: Proceedings of the International Gas Turbine Congress 2003, 2003, Paper No. IGTC2003-TS-059, p. 7. November 2-7, 2003, Japan, Tokyo.

[32] I. Celik, U. Ghia, P. Roache, C. Freitas, H. Coleman, P. Raad, Procedure

for Estimation and Reporting of Uncertainty Due to Discretization in CFD Applications, Journal of Fluids Engineering 130 (7) (2008) Article ID 078001, 4 pages. doi:10.1115/1.2960953.

[33] D. Hagelstein, K. Hillewaert, E. A. Van den Braembussche, R.A. and, R. Keiper, M. Rautenberg, Experimental and Numerical Investigation of the Flow in a Centrifugal Compressor Volute, Journal of Turbomachinery 122 (1) (2000) 22–31. doi:10.1115/1.555423.

[34] Z. Sun, C. Tan, D. Zhang, Flow Field Structures of the Impeller Backside Cavity and Its Influences on the Centrifugal Compressor, in: Proceedings of ASME Turbo Expo 2009: Power for Land, Sea and Air, Vol. 7, 2009, pp. 1349–1360, Paper No. GT2009-59879. June 8-12, 2009, Orlando, Florida, USA. doi:10.1115/GT2009-59879.

[35] S. Bareiß, D. M. Vogt, E. Chebli, Investigation on the Impact of Circumferential Grooves on Aerodynamic Centrifugal Compressor Performance, in: Proceedings of ASME Turbo Expo 2015: Turbine Technical Conference and Exposition, 2015, Paper No. GT2015-42211, p. 11. June 15–19, 2015, Montreal, Canada. doi:10.1115/GT2015-42211.

[36] F. J. Wiesner, A New Appraisal of Reynolds Number Effects on Centrifugal Compressor Performance, Journal of Engineering for Gas Turbines and Power 101 (3) (1979) 384–392. doi:10.1115/1.3446586.

[37] M. Casey, The Effects of Reynolds Number on the Efficiency of Centrifugal Compressor Stages, Journal of Engineering for Gas Turbines and Power 107 (1985) 541–548. doi:10.1115/1.3239767.

[38] M. Heß, P. Pelz, On Reliable Performance Prediction Of Axial Turbomachines, in: Proceedings of ASME Turbo Expo 2010: Power for Land, Sea and Air, Vol. 7, 2010, pp. 139–149, Paper No. GT2010-22290. June 14-18, 2010, Glasgow, UK. doi:10.1115/GT2010-22290.

[39] P. Pelz, S. Stonjek, The Influence of Reynolds Number and Roughness on the Efficiency of Axial and Centrifugal Fans - a Physically Based Scaling Method, Journal of Engineering for Gas Turbines and Power 135 (5) (2013) Article ID 052601, 8 pages. doi:10.1115/1.4022991.

[40] K. Isomura, M. Murayama, S. Teramoto, K. Hikichi, Y. Endo, S. Togo, S. Tanaka, Experimental Verification of the Feasibility of a 100 W Class Micro-Scale Gas Turbine at an Impeller Diameter of 10 mm, Journal of Micromechanics and Microengineering 16 (9) (2006) S254–S261. doi:10.1088/0960-1317/16/9/S13.

[41] S. Kang, M. Matsunaga, J. Johnston, H. Tsuru, T. Arima, F. Prinz, Micro-Scale Radial-Flow Compressor Impeller Made of Silicon Nitride - Manufacturing and Performance, in: Proceedings of ASME Turbo Expo 2003: Power for Land, Sea, and Air, Vol. 3, 2003, pp. 779–788, Paper No. GT2003-38933. June 16-19, 2003, Atlanta, Georgia, USA. doi:10.1115/GT2003-38933.

[42] D. Eckardt, Detailed Flow Investigations Within a High-Speed Centrifugal Compressor Impeller, Journal of Fluids Engineering 98 (3) (1976) 390–399. doi:10.1115/1.3448334.

[43] J. D. Denton, Loss Mechanisms in Turbomachines, Journal of Turbomachinery 115 (1993) 621–656. doi:10.1115/1.2929299.

[44] K. Vogel, R. S. Abhari, A. Zemp, Experimental and Numerical Investigation of the Unsteady Flow Field in a Vaned Diffuser of a High-Speed Centrifugal Compressor, Journal of Turbomachinery 137 (7), Article ID 071008, p. 9. doi:10.1115/1.4029175.

[45] T. Turunen-Saaresti, A. Jaatinen, Influence of the Different Design Parameters to the Centrifugal Compressor Tip Clearance Loss, Journal of Turbomachinery 135 (2013) Article ID 011017, 6 pages. doi:10.1115/1.4006388.

[46] M. Kaneko, H. Tsujita, T. Hirano, Numerical Analysis of Flow in Ultra Micro Centrifugal Compressor -Influence of Meridional Configuration, Journal of Thermal Science 22 (2) (2013) 111–116. doi:10.1007/s11630-013-0600-7.

[47] Y. Ma, G. Xi, Effects of Reynolds Number and Heat Transfer on Scaling of a Centrifugal Compressor Impeller, in: Proceedings of the ASME Turbo Expo 2010: Power for Land, Sea and Air, Vol. 5, 2010, pp. 565–572, Paper No. GT2010-23372. June 14-18, 2010, Glasgow, UK. doi:10.1115/GT2010-23372.

[48] S. Burguburu, A. Fourmaux, J. Guidez, Numerical Design of an Ultra Micro-Compressor and Micro-Turbine, in: Proceedings of XIX International Symposium on Air Breathing Engines (ISABE 2009), 2009, pp.

1529 – 1536, Paper No. ISABE-2009-1306. September 7-11, 2009, Montreal, Canada.

[49] R. Langtry, F. Menter, Transition Modeling for General CFD Applications in Aeronautics, in: 43rd AIAA Aerospace Sciences Meeting and Exhibit, 2005, Paper No. AIAA 2005-522. January, 10 – 13, 2005, Reno, Nevada. doi:10.2514/6.2005-522.

[50] L. Galloway, S. Spence, S. Kim, D. Rusch, K. Vogel, R. Hunziker, An Investigation of the Stability Enhancement of a Centrifugal Compressor Stage Using a Porous Throat Diffuser, in: Proceedings of the ASME Turbo Expo 2017: Turbomachinery Technical Conference and Exposition, 2017, Paper No. GT2017-63071, 14 pages. June 26–30, 2017, Charlotte, NC, USA. doi:10.1115/GT2017-63071.